Spectrochimica Acta Part B 77 (2012) 44–51

Contents lists available at SciVerse ScienceDirect

Spectrochimica Acta Part B

journal homepage: www.elsevier.com/locate/sab

Standardless quantification by parameter optimization in electron probe microanalysis

Silvina P. Limandri [a,b], Rita D. Bonetto [c,d], Víctor Galván Josa [a,b], Alejo C. Carreras [a,b], Jorge C. Trincavelli [a,b,*]

[a] Instituto de Física Enrique Gaviola (IFEG), CONICET, Argentina
[b] Facultad de Matemática, Astronomía y Física, Universidad Nacional de Córdoba, Medina Allende s/n, (5016) Córdoba, Argentina
[c] Centro de Investigación y Desarrollo en Ciencias Aplicadas Dr. Jorge Ronco (CINDECA), CONICET, 47 Street #257, (1900) La Plata, Argentina
[d] Facultad de Ciencias Exactas, Universidad Nacional de La Plata, 1 and 47 Streets (1900) La Plata, Argentina

ARTICLE INFO

Article history:
Received 19 June 2012
Accepted 24 August 2012
Available online 5 September 2012

Keywords:
Standardless quantification
EPMA
Parameter optimization
EDS

ABSTRACT

A method for standardless quantification by parameter optimization in electron probe microanalysis is presented. The method consists in minimizing the quadratic differences between an experimental spectrum and an analytical function proposed to describe it, by optimizing the parameters involved in the analytical prediction. This algorithm, implemented in the software POEMA (Parameter Optimization in Electron Probe Microanalysis), allows the determination of the elemental concentrations, along with their uncertainties. The method was tested in a set of 159 elemental constituents corresponding to 36 spectra of standards (mostly minerals) that include trace elements. The results were compared with those obtained with the commercial software GENESIS Spectrum® for standardless quantification. The quantifications performed with the method proposed here are better in the 74% of the cases studied. In addition, the performance of the method proposed is compared with the first principles standardless analysis procedure DTSA for a different data set, which excludes trace elements. The relative deviations with respect to the nominal concentrations are lower than 0.04, 0.08 and 0.35 for the 66% of the cases for POEMA, GENESIS and DTSA, respectively.

1. Introduction

Electron probe microanalysis (EPMA) is a non destructive technique for chemical characterization, based on the analysis of the X-ray spectrum emitted when a sample is irradiated by an electron beam. This technique is applied in a great number of fields, such as materials science, metallurgy, geology, archeology, art, and forensics. Electron probe microanalysis gives qualitative information about the elements present in the sample straightforwardly. However, the quantitative determination of the chemical composition is not always an easy task for the analyst.

Conventional quantification methods in EPMA involve the use of standards. The characteristic line intensity emitted by each element of an unknown sample is compared with the corresponding intensity emitted from a standard. As a rough approximation, the intensity ratio, known as *k* ratio, may be taken as proportional to the mass concentration of the considered element. These ratios must be corrected by matrix effects, i.e., effects related to the other elements present in the sample and in the standard. Thus, production, absorption and enhancement of the characteristic radiation are taken into account. There exist two methods to perform these corrections: the models based on the *ZAF* factors and on the ionization distribution function $\phi(\rho z)$ [1].

During the last fifty years, the corrections to the *k* ratio have been studied in different kind of samples. The results of these investigations lead to reduce significatively the relative errors associated to the elemental concentrations. When a wavelength dispersive spectrometer (WDS) is used, the relative uncertainties are about 5% for major and minor elements, i.e., with concentrations greater than 10% and between 1 and 10%, respectively, and somewhat greater for trace elements (concentrations lower than 1%) [2]. In the special case of mineral samples, the relative errors of the elemental concentrations become lower than 2% in most of the situations [3].

One of the advantages related to the use of standards is that several atomic and experimental parameters cancel out in the *k* ratio. Unfortunately, when several standards are used, measurements can take too much time; in addition, sometimes the appropriate set of standards is not available. In the last decades, there has been an increasing interest in the development of accurate standardless methods for chemical quantification. Currently, standardless routines are included in commercial energy dispersive spectrometers (EDS) [2], but only as semiquantitative tools.

The standardless quantification methods can be classified in two groups: the ones based on first principles and those involving databases. In the latter, a database of characteristic intensities is created from a set of experimental spectra, usually monoelemental standards

* Corresponding author at: Facultad de Matemática, Astronomía y Física, Universidad Nacional de Córdoba, Medina Allende s/n, (5016) Córdoba, Argentina. Tel.: +54 351 4334051; fax: +54 351 4334054.
E-mail address: trincavelli@famaf.unc.edu.ar (J.C. Trincavelli).

0584-8547/$ – see front matter © 2012 Elsevier B.V. All rights reserved.
http://dx.doi.org/10.1016/j.sab.2012.08.003

measured under different excitation conditions. These intensities are mathematically interpolated for elements or conditions not measured in order to complete the database, which is used to determine the k ratios. The reliability of this kind of methods lies on the completeness of the database and leads to inaccurate results when the interpolation is not adequate. On the other hand, the development of a standardless algorithm based on first principles, although presents a number of difficulties, could be a more general characterization tool.

The main problem in the development of standardless quantitative algorithms based on first principles is that the physics underlying generation, propagation and detection of X-rays must be properly known. Therefore, adequate descriptions of characteristic radiation, bremsstrahlung, and detection artifacts are required. The influence of these artifacts is avoided in the so-called peak-to-background algorithms [4,5], although they rely on the rough assumptions that both characteristic and bremsstrahlung photons are originated in the same region of the sample and that bremsstrahlung is emitted isotropically. A proper description of the depth distribution of the characteristic X-ray generation is a key issue in the development of a fundamental standardless quantitative algorithm. It can be described by means of two methods: Monte Carlo simulations [6] and analytical approximations [7,8], some of which are obtained from the parameterization of experimental determinations. The Monte Carlo method is more precise but it requires a long computational time. Analytical approximations have been intensively studied, reaching an acceptable level of accuracy for most of the cases [9].

The main sources of error in standardless procedures based on first principles are related to the uncertainties associated with the measured intensities, the knowledge of atomic parameters and the description of the detection efficiency in the low energy region. One of the most influential atomic parameters involved is the ionization cross section Q. Realistic models for the description of Q, for instance, those based on the distorted-wave first-order Born approximation (DWBA), present uncertainties around 5% [10].

In the present work, the performance of the standardless quantification algorithm in EPMA, implemented in the software POEMA, is assessed for a set of samples. The original version of the program [11] was completed and improved by updating the database used for K-, L- and M-relative transition probabilities [12–14], for K- and L-ionization cross sections [10] and for $K\alpha$ and $K\beta$ satellite lines [15,16]. In addition, the model used to describe the bremsstrahlung [17,18] and a model for the line shape for EDS [19] were improved and implemented in POEMA. A routine for processing WDS spectra was also included, with a proper description for the line shape [20] and detector efficiency [21]. Finally, the effects produced in a spectrum by a possible oxidation layer and a conductive coating film deposited on the sample were included in the program [22]. In order to test the goodness of the algorithm, 36 spectra of standards (mostly minerals) measured with an EDS, were processed and the compositions of the samples were obtained. The deviations of the 159 concentrations obtained with POEMA relative to the nominal values were analyzed. These results were compared with the ones obtained by the commercial software GENESIS Spectrum® (EDAX) for the same set of spectra, and with the results reported by Newbury et al. [2] for a different set of samples.

2. Experimental

X-ray emission spectra of the set of standards SPI #02753-AB were measured with an EDAX Genesis 2000 energy dispersive spectrometer, attached to a LEO 1450VP scanning electron microscope. The measured standards were: anhydrite, apatite, bustamite, calcite, diopside, dolomite, kaersutite, olivine, pentlandite, tugtupite, plagioclase, willemite, quartz, haematite, rutile, sphalerite, skutterudite, albite, almandine, biotite, BN, chlorite, Cr_2O_3, cuprite, spodumene, fluorite, GaAs, pyrope garnet, jadeite, magnetite, Ni_2Si, obsidian, periclase, pyrite, rhodonite, and sanidine. The EDS has a SUTW Sapphire Si(Li) detector with ultrathin polymer window with aluminum ohmic contact. Spectra were induced by an incident electron beam of 15 keV for all the samples, except for olivine, pentlandite and willemite, for which 20 keV was used. The take-off angle ranged between 29.6 and 33.4°.

All the samples were quantified with the home-made software POEMA (see Section 3) and with the commercial program GENESIS Spectrum® in standardless mode. In the latter, the k factors are calculated as the ratios between the measured peak intensity and the intensity corresponding to the pure element, calculated from first principles. This ratio is then corrected by matrix effects (ZAF corrections) to take into account the influence of the other elements in the sample. The program allows the user to perform corrections related to the detector efficiency and to the carbon conductive coating of the sample, whose thickness must be known a priori.

All the standards used are embedded in a 25 mm diameter disk, polished and coated with a carbon layer. The spectra analyzed in this work were measured between 2006 and 2011. The set of standards was re-polished and re-coated in 2010, thus, the carbon coating thickness has not been necessarily the same before and after this year.

3. Spectral processing

The optimization method implemented for spectral processing consists in minimizing the quadratic differences between the experimental spectrum to be fitted and an analytical function proposed to describe it, by optimizing the parameters involved in the analytical prediction [11]. The quantity to be minimized can be written as:

$$\chi^2 = \frac{1}{N_c - N_p}\sum_{i=1}^{N_c}\frac{\left(\tilde{I}_i - I_i\right)^2}{I_i} \tag{1}$$

where I_i and $\tilde{I}_i$ are, respectively, the experimental and calculated intensities for the energy E_i corresponding to channel i, N_c is the total number of channels and N_p is the number of parameters to be refined. Thus, the sample composition is obtained as a result of the optimization procedure, by the refinement of the concentrations and also of certain instrumental parameters. The refinement procedure must be carried out through a cautious sequence of minimization steps in order to get the best fit of the experimental spectrum.

The function $\tilde{I}_i$ describes the entire spectrum, i.e., all the peaks and the bremsstrahlung, taking into account the generation and absorption of radiation within the specimen, enhancement by secondary fluorescence, detection artifacts and spectrometer efficiency. The calculated intensity at the energy E_i can be written as:

$$\tilde{I}_i = B(E_i) + \sum_{j,q} P_{j,q} H_{j,q}(E_i) + D(E_i) \tag{2}$$

where $B(E_i)$ accounts for the bremsstrahlung contribution, $P_{j,q}$ is the peak intensity of the line q of the element j, $H_{j,q}$ is a modified Gaussian function that describes the corresponding line profile (see Section 3), and the function $D(E_i)$ takes into account the contribution of escape peaks, sum peaks and the Si peak generated within the detector.

3.1. Bremsstrahlung

The expression for $B(E_i)$ as a function of the photon energy E_i is given by [18]:

$$\begin{aligned} B(E_i) = {} & \sqrt{\bar{Z}}\,\frac{(E_0 - E_i)}{E_i}\,\alpha A R \varepsilon(E_i) \\ & \times\left(-73.90 - 1.2446E_i + 36.502\ln Z + \frac{148.5E_0^{0.1293}}{\bar{Z}}\right) \\ & \times\left[1 + (-0.006624 + 0.0002906E_0)\frac{\bar{Z}}{E_i}\right] \end{aligned} \tag{3}$$

where the energy is in keV, $\bar{Z}$ is the mass weighted average atomic number, E_0 is the incident electron energy, α is a constant proportional to the number of incident electrons, A is the absorption correction, R accounts for intensity losses due to backscattered electrons, and ε is the spectrometer efficiency.

3.2. Characteristic line intensities

The detected characteristic intensity $P_{j,q}$ of the line q, of the element j, can be expressed as:

$$P_{j,q} = \beta C_j \sigma^X_{j,s} p_{j,q} (ZAF)_{j,q} \varepsilon\left(E_{j,q}\right) \tag{4}$$

where β is a constant proportional to the number of incident electrons, C_j is the mass concentration of the element j in the sample, Z, A and F are the matrix correction factors related to X-ray generation, absorption and fluorescence enhancement in the specimen, respectively; $p_{j,q}$ is the relative transition probability for the line q of the element j, $E_{j,q}$ is the energy of this transition and $\sigma^X_{j,s}$ is the X-ray production cross section for the corresponding s atomic shell at energy E_0. The latter is defined for the K-shell as the product of the ionization cross section and the fluorescence yield, which were taken from the data published by Campos et al. [10] and Hubbell [23], respectively.

Regarding Z, A, and F corrections, a model for the ionization distribution function $\phi(\rho z)$ previously developed [24], and based on the description given by Packwood and Brown [25], was used in the present calculations.

3.3. Peak shape

The detection system response for a given characteristic line is a broadened peak, with a Gaussian shape to a first approximation, whose width is a function of the photon energy and is related to the electronic noise of the amplification process and to the Fano factor [11]. However, the characteristic X-ray peaks obtained using a Si(Li) detector exhibit an asymmetric shape mainly due to an effect of incomplete charge collection in the detector. The expression used in the spectral processing algorithm to describe the line profile of the characteristic peaks was developed in a previous work [19], and can be written as:

$$H_{j,q}(E_i) = M\left[G_{j,q}(E_i) + T_{j,q}(E_i)\right] \tag{5}$$

where M is a normalization factor defined so that the integral of $H_{j,q}(E_i)$ is equal to unity, $G_{j,q}(E_i)$ is a normalized Gaussian function characterized by a width $\sigma_{j,q}$, centered at the characteristic energy $E_{j,q}$ and $T_{j,q}(E_i)$ is an exponential tail convoluted with a Gaussian and depends on two parameters: the width $\beta_{j,q}$ and the height $t_{j,q}$.

The T function presented in the original article [19] was not normalized, because it was not necessary for that study. In the present work, the expression for the T function was properly scaled:

$$T_{j,q}(E_i) = \frac{1}{2} t_{j,q} \exp\left(\sigma^2_{j,q}/2\beta^2_{j,q}\right) \exp\left[\left(E_i - E_{j,q}\right)/\beta_{j,q}\right] \times \operatorname{erfc}\left(\frac{E_i - E_{j,q}}{\sqrt{2}\sigma_{j,q}} + \frac{\sigma_{j,q}}{\sqrt{2}\beta_{j,q}}\right) \tag{6}$$

The knowledge of the dependence of the peak asymmetry with the photon energy is very important to achieve an adequate spectral deconvolution, particularly when there is a strong overlapping between intense and weak peaks that affects the accuracy of quantitative analysis.

In this work, the behavior of $t_{j,q}$ and $\beta_{j,q}$ with the characteristic photon energy, for elements with $Z<15$, was taken into account by fitting analytical functions, which were used to describe the peak asymmetry in the quantification procedure. These analytical expressions were derived from the values of $t_{j,q}$ and $\beta_{j,q}$ obtained for several characteristic energies $E_{j,q}$ by processing the spectra of the following mineral standards: willemite, anhydrite, olivine, calcite, dolomite, diopside, plagioclase, tugtupite and kaersutite. In this procedure, the nominal concentrations and the characteristic thicknesses of the detector layers provided by the manufacturer were used, and the thickness of the carbon coating Δx_C was optimized along with $t_{j,q}$ and $\beta_{j,q}$.

It was previously shown [19] that the relative area of the asymmetric correction presents a jump at the energy of the silicon absorption edge. For this reason, to take into account this discontinuity, the parameters $t_{j,q}$ and $\beta_{j,q}$ for K peaks corresponding to elements with $Z>14$, were optimized together with the elemental concentrations in the quantification procedure, when necessary.

3.4. Detection efficiency

The detection efficiency ε is the fraction of the X-rays emitted by the sample that are actually registered. In order to determine ε, it must be born in mind that to be registered, the photon must arrive to the detector active region passing through several layers: the polymer window (PW), the aluminum ohmic contact and the so-called dead layer (DL), where detection is not possible. It must be also considered that the incident photon can go across the active region of the detector and not be detected.

According to a previous study [21], the detector efficiency can be expressed as:

$$\varepsilon = \exp\left[-(\mu\rho x)_{PW}\right]\exp\left[-(\mu\rho x)_{Al}\right]\exp\left[-\mu_{Si}\rho_{Si}x_{DL}\right] \times\left\{1-\exp\left[-\mu_{Si}\rho_{Si}x_{det}\right]\right\} \times \left[0.77 + 0.23\exp\left(-\mu_{Si}\rho_{Si}x_{Grid}\right)\right]\frac{\Delta\Omega}{4\pi} \tag{7}$$

where $(\mu\rho x)_{PW}$ and $(\mu\rho x)_{Al}$ are the products of the mass absorption coefficient, density and thickness of the polymer window and the aluminum ohmic contact, respectively. x_{Grid} is the thickness of the silicon supporting grid, μ_{Si} and ρ_{Si} are the mass absorption coefficient and density of silicon. The first factor in the right-hand member of Eq. (7) is related to the attenuation of the incident photons in the polymer window, the second one accounts for the photon losses in the aluminum ohmic contact, the third one takes into account the absorption in the dead layer, the fourth one is the probability that a photon be absorbed in the detector active region, and the fifth one takes into account the fraction of photons arriving to the detector either through the open area or across the silicon support grid, which represents a 23% of the total detector area for the system used.

The thickness of the detector dead layer was determined by processing the tugtupite, plagioclase, dolomite, diopside, kaersutite, willemite and calcite spectra, in an energy region where the efficiency corrections are important (between 0.17 and 2.2 keV). The asymmetry parameters ($t_{j,q}$ and $\beta_{j,q}$) for elements with $Z<15$, and the dead layer and carbon coating thicknesses were then determined by an iterative process. After convergence, the dead layer thickness obtained was $x_{DL} = 32 \pm 3$ nm and the average of carbon coating thicknesses for these samples was $\Delta x_C = 31 \pm 6$ nm.

3.5. Fitting methodology for quantification

The optimization method implemented in the software POEMA requires following certain minimization steps, checking the physical meaning of the results obtained each time. In order to avoid local minima it is convenient to begin from an adequate estimation of the values of the parameters to be refined. In the present work, the initial values of the concentrations were taken as the intensities of the corresponding characteristic peaks normalized to unity. Characteristic energies given by Bearden [26] were used, whereas the relative transition probabilities for decays to K and L shells were taken from the articles published by Limandri et al. [15] and Pia et al. [27].

Certain global parameters were initially fitted in a wide region of the spectra involving all the peaks: the scale factors for background and for characteristic peaks (α and β), the calibration parameters (spectrometer gain and zero) and parameters related to the peak width (electronic noise and Fano factor). Then, the elemental concentrations were also refined along with the carbon coating thickness, using the dead layer thickness obtained as explained in the previous subsection.

All the mass concentrations were obtained from the fitting of *K* peaks due to the large uncertainties of the atomic parameters related to *L* and *M* atomic shells, such as radiative transition probabilities, fluorescence yields and, particularly, Coster–Kronig transition probabilities [28].

A few spectra deserve some particular remarks. A case particularly difficult was the rutile spectrum, due to the strong overlapping between Ti-*L* and the O-*K* lines. The deconvolution was very complicated because the detector resolution did not allow us to distinguish the different Ti-*L* lines and, in addition, the corresponding relative transition probabilities are not known with good precision. The optimization procedure began from *L* relative transition probabilities obtained by extrapolation of the data given by Pia et al. [27]. The spectrum was fitted initially in a wide region (between 0.1 and 6 keV), refining the β constant for *K* and *L* peaks, the O and Ti concentrations, the parameters related to calibration and peak width, and the carbon coating thickness (starting from the average of the values obtained as explained in Section 3.4). Then, the transition probabilities were optimized in a region centered around the Ti-*L* peaks. These two optimization steps were repeated until the convergence was achieved. A similar method was applied for the hematite spectrum.

As mentioned previously, the carbon coating thickness was refined during the quantification procedure, but two exceptions were made for minerals containing carbon (calcite and dolomite). In these cases, the carbon thickness was set according to the average of the values obtained from the other quantifications (corresponding to spectra measured in the same period than those spectra).

3.6. Estimation of uncertainties

After convergence is achieved, the errors in the concentrations were estimated by performing an additional optimization step, which involves the global constants and the concentrations in a wide spectral region that includes all the characteristic peaks of interest, provided the correlation between the global parameters and the concentrations were less than 0.9. Otherwise, the global constants highly correlated were fixed and the remaining parameters were refined.

For low statistic peaks, where certain parameters were optimized in narrow spectral regions, the errors of the corresponding concentrations were estimated by considering only the uncertainties related to experimental statistics, i.e., assuming that errors due to matrix corrections and to the other parameters involved in the prediction of the spectrum are negligible.

The errors affecting the quantification process (with or without standards) can be classified into five groups [29]:

1. Errors associated with counting statistics.
2. Errors associated with the sample and its preparation (e.g. dirty or irregular surfaces, inhomogeneities, etc.).
3. Errors in the measuring process (e.g. fluctuations in the beam current, uncertainties in the excitation potential, etc.) and in data processing (e.g. determination of characteristic and background intensities).
4. Errors associated with the databases used for the physical parameters involved in the quantification routine (e.g. backscattered electron coefficients, surface ionization, fluorescence yields, ionization cross sections, transition probabilities, attenuation coefficients, etc.).
5. Errors associated with the models used for the description and correction of the measured characteristic intensities (e.g. matrix corrections, bremsstrahlung prediction, correction for the conductive coating, detector efficiency, etc.).

In the case of standardless quantification of major and minor elements, the greater error sources correspond to groups 4 and 5. For trace elements, instead, the uncertainties associated with counting statistics (group 1) are usually the most important ones.

The program POEMA estimates the uncertainties in the obtained parameters by propagating the errors associated with counting statistics, given by the square root of the number of counts, through the function that describes the X-ray spectrum. This algorithm of error propagation, roughly assumes that the analytical models used have no error. In order to include other sources of error, the relative error determined by the program is summed in quadrature with the relative uncertainty estimated for the detector efficiency correction and with the relative errors of certain atomic parameters. Efficiency uncertainties between 0.5% and 15% (depending on the energy of the analyzed line) were obtained by assuming relative errors of 10% in the detector characteristic thicknesses and the uncertainties estimated by Chantler et al. for the mass absorption coefficients [30]. Regarding the errors in the atomic parameters, the most influential ones are: the error in the fluorescence yields, which is around 2% for *K* lines [31–33], and the error in the ionization cross section, estimated as 5% for *K* lines. This last estimation was performed from the analysis of a set of experimental determinations of ionization cross sections in thin targets, where the errors in the target thickness, in the intrinsic detection efficiency and in the solid angle subtended by the detector were considered [35].

Another problem inherent to error estimation is that when parameters very correlated are refined together, the estimated uncertainties are too large. In addition, the assignation of errors performed by the software POEMA depends only on the parameters refined in the last optimization, regardless the whole process which involves several optimization steps. A more detailed description about this issue can be found elsewhere [34]. The uncertainties estimated by POEMA for the concentrations obtained in the present work were below 40, 10 and 5% in most of the cases, for trace, minor and major constituents, respectively.

4. Results and discussion

In Fig. 1, examples of the fits obtained are shown for kaersutite (Fig. 1a) and rutile (Fig. 1b) spectra. These spectra were chosen because they illustrate typical difficulties found in the whole set studied: kaersutite is a mineral with many elements and rutile is a binary sample (Ti–O), one of whose elements (Ti) presents intense *L* lines in the region of the O-*K*α peak.

The quantifications performed by the GENESIS Spectrum® software were done by using the values of the detector parameters set by default in that program. Two different correction factors were obtained to take into account the carbon coating in the quantifications performed by GENESIS before and after 2010. It was necessary to carry out these two determinations because the standards had been re-coated in 2010, as mentioned in Section 2. The determinations for the carbon coating correction factors were performed in three spectra representative of the measurements done before 2010, corresponding to tugtupite, dolomite and diopside, and in three spectra measured in 2011: albite, almandine and bustamite. These samples were quantified by using the software GENESIS with different carbon coating correction factors, to determine the optimal factor that produced the concentration values closest to the nominal ones. The correction factors obtained averaging the three values corresponding to each group were 12 and 16 for the spectra measured before 2010 and during 2011, respectively. Even when it is known that these factors are related to the conductive coating thickness, it is not clear from the user manual which is exactly that relation.

In all the cases, for nominal and calculated values, the concentrations of the elements detected were normalized to unity. In order to

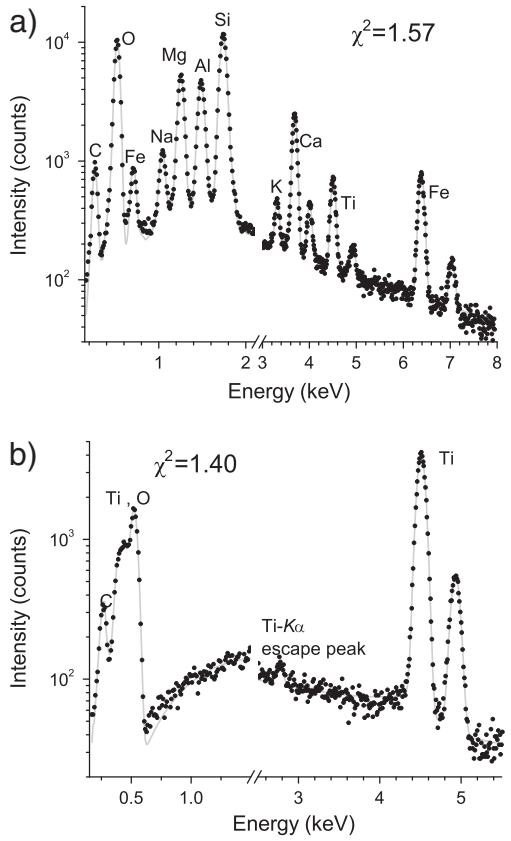

Fig. 1. Experimental and fitted spectra for a) kaersutite and b) rutile. Dots: experimental data; lines: fitting performed by means of the software POEMA.

compare the quality of the programs, the determinations were carried out by elements, i.e., no stoichiometric relation was used to link the concentration of different elements, even for elements with low energy characteristic lines, such as C and O, except for H, Li and Be, which do not present detectable characteristic lines. The possibility to analyze elements individually allows the user to perform quantification even when stoichiometry is not known.

Tables 1 and 2 show the results of the quantifications performed. As can be observed, the 74% of the concentrations determined with POEMA, are closer to the nominal values than those obtained by the EDAX commercial software. In Table S1 (Appendix), the absolute and relative differences between each method and the nominal values are also shown.

The relative differences of concentrations obtained with both programs with respect to the nominal values, $\Delta C/C$, are shown in the histograms of Fig. 2. The centers of the histograms are placed at 2.4% and 0.04%. In addition,106 of the 159 cases studied present $\Delta C/C$ values lower than 0.08 and 0.04 for the quantifications performed by GENESIS and POEMA, respectively, showing a better performance of the latter. It must be noted that these relative differences are of the same order of magnitude as the uncertainties estimated in the present work.

In Fig. 2a, the results published by Newbury et al. [2,8] using the quantification software DTSA [36], were also included. Basically, DTSA program calculates *k* ratios, where the intensity corresponding to the pure standards is predicted from the first principles involving different models for the *K*-, *L*- and *M*-shell ionization cross sections. Newbury et al. [2] concluded from a particular set of samples that standardless methods are not reliable. For this reason, even when the particular set of samples and experimental conditions used for DTSA quantifications are different to the ones used in this work, the comparison among the three methods is of interest to decide if the performance of standardless methods has changed with the improvement of X-ray detection spectrometers and quantification procedures. It must be emphasized that the set of spectra used in the present paper has a higher degree of difficulty to perform quantification than the set used by Newbury et al. Particularly, the samples quantified with DTSA were a set of compounds with a well known stoichiometric relation. The determinations were carried out avoiding deconvolution problems by choosing the samples with negligible peak interference in almost all the cases [2]. These authors mostly worked with *K* lines, although they included some *L* and *M* lines in their study. It is important to note that in that work, only elements with concentrations greater than 1% were considered, in other words, trace elements were not taken into account. In addition, light elements such as oxygen were quantified by means of the stoichiometric relation. The lower characteristic energy analyzed by Newbury et al. [2] was 0.93 keV, i.e., the Cu-*Lα* line energy. As can be seen from Fig. 2a, the histogram corresponding to their data is centered around −0.71%, with a standard deviation of 36%.

If major, minor and trace elements are taken into account, the 51% and the 72% of the concentrations determined with GENESIS and POEMA, respectively, deviate from the nominal concentrations less than 5%. As expected, both programs present the major relative differences for trace elements. This fact is inherent to all the EPMA analytical methods, with or without standards. This difficulty is mainly due to the uncertainties related to measurement statistics, which are important for weak peaks. In such cases, the differences from the nominal concentrations can reach 150% and 200% for POEMA and GENESIS, respectively. Nevertheless, when trace elements are disregarded, the spread of the calculated concentrations is markedly reduced (see Fig. 2b) and the maximum deviation decreases to 32% for both programs. In this last case, the 93% of our results present values $\Delta C/C$ between −10% and 10%, which is greater than the 68% and than the 25% obtained with GENESIS and DTSA (for a different set of samples), respectively. On the other hand, even when boron and nitrogen nominal concentrations in the BN spectrum are greater than 40%, both programs, GENESIS and POEMA, have difficulties in the quantification of these elements. This fact occurs because the B-*K* peak is placed at a very low energy (0.18 keV), where the detector efficiency is not known with a good precision. Furthermore, the matrix corrections could not be well predicted for the two elements involved; particularly for boron.

Although the GENESIS software has the possibility to make specific corrections for B, C and N, the use of samples of known composition similar to the unknown sample is required in a preliminary step, i.e., the use of standards becomes necessary. The deviations of the concentrations from the nominal values for oxygen (major element in all the studied cases) determined with POEMA were less than 6% for 27 of the 28 spectra involving this element. Therefore the estimation for the detection efficiency and the atomic parameters involved in this software, are properly described for oxygen. The quantification of carbon is more complicated, particularly due to the contribution of the conductive carbon coating. Only two samples containing carbon were quantified (calcite and dolomite). In the case of calcite, the performance of POEMA was better, while for dolomite, GENESIS led to better results. The most unfavorable cases are indicated in Fig. 2b).

If the effects caused by the conductive coating were not taken into account, important errors could arise in the quantification procedure, mainly for light elements, whose characteristic photons are strongly absorbed by carbon. For instance, the oxygen concentration obtained with POEMA for olivine was 0.438, which is very close to the nominal value (0.439), while if this sample is quantified neglecting the influence of the conductive cover, the concentration would result to 0.410.

Unlike GENESIS software, POEMA allows the optimization of the carbon coating mass thickness along with the concentrations. The mean values obtained for the coating thickness, assuming a carbon density of 2.27 g/cm^3 were (29 ± 4) nm and (83 ± 7) nm for the spectra measured before 2010 and for the ones acquired during 2011, respectively. Nevertheless, it is important to remark that, according to Reed [37], the density of the deposited carbon film can be quite less than this value.

Table 1
Mass concentrations obtained with the present method and with the commercial software GENESIS by EDAX compared to the nominal values. Numbers in parentheses are the estimated uncertainties in the two last digits.

Sample Δx_C (nm)	El.	Nom.	EDAX	POEMA
Anhydrite[a]	O	0.4701	0.4833	0.476(46)
35 (2)	S	0.2355	0.2355	0.236(13)
	Ca	0.2944	0.2812	0.288(17)
Calcite[a]	C	0.1202	0.0921	0.127(20)
	O	0.4799	0.5036	0.475(46)
	Ca	0.3999	0.4043	0.398(22)
Diopside[a]	O	0.4439	0.436	0.445(43)
32 (1)	Mg	0.1125	0.12	0.1117(65)
	Si	0.2593	0.273	0.264(15)
	Ca	0.1843	0.1673	0.180(10)
Dolomite[a]	C	0.1306	0.1124	0.171(27)
	O	0.5208	0.5173	0.491(47)
	Mg	0.1308	0.1499	0.1244(72)
	Ca	0.2178	0.2204	0.214(12)
Kaersutite[a]	O	0.4309	0.4396	0.430(42)
29.6 (7)	Na	0.0182	0.0186	0.0187(41)
	Mg	0.0762	0.0817	0.0788(46)
	Al	0.0658	0.0697	0.0685(40)
	Si	0.1886	0.1953	0.194(11)
	K	0.0098	0.0082	0.00799(54)
	Ca	0.0831	0.0743	0.0808(46)
	Ti	0.0304	0.0291	0.0310(19)
	Mn	0.0014	0.0012	0.0011(10)
	Fe	0.0957	0.0824	0.0893(51)
Olivine[a]	O	0.4393	0.4343	0.438(42)
31.5 (9)	Mg	0.3044	0.3139	0.304(18)
	Si	0.1946	0.1975	0.194(11)
	Fe	0.0587	0.0518	0.0611(36)
	Ni	0.003	0.0025	0.00308(44)
Pentlandite[a]	S	0.3301	0.3347	0.319(18)
29 (1)	Fe	0.3077	0.3026	0.298(17)
	Co	0.001	–	0.00197(61)
	Ni	0.3612	0.3627	0.381(22)
Plagioclase[a]	O	0.4717	0.4738	0.466(45)
26.6 (2)	Na	0.0324	0.0345	0.0320(19)
	Al	0.1513	0.1555	0.1552(90)
	Si	0.2539	0.2525	0.257(14)
	K	0.0034	0.0024	0.00251(88)
	Ca	0.0845	0.0783	0.0842(49)
	Fe	0.0029	0.003	0.0033(13)
Tugtupite[a]	O	0.4185	0.4151	0.417(40)
31.7 (5)	Na	0.2004	0.209	0.198(11)
	Al	0.0588	0.0597	0.0587(35)
	Si	0.2449	0.2481	0.250(14)
	Cl	0.0773	0.0681	0.0773(45)
Willemite[a]	O	0.294	0.3006	0.309(31)
35 (1)	Si	0.1313	0.1395	0.1154(90)
	Mn	0.0373	0.0382	0.0330(19)
	Zn	0.5374	0.5217	0.543(31)
Quartz[a]	O	0.5326	0.5147	0.515(50)
25(1)	Si	0.4674	0.4853	0.485(27)
Hematite[a]	O	0.3006	0.3153	0.287(28)
25 (1)	Fe	0.6994	0.6847	0.713(40)
Rutile[a]	O	0.4006	0.4119	0.400(39)
23 (1)	Ti	0.5994	0.5881	0.600(34)
Sphalerite	S	0.3292	0.3172	0.319(19)
74 (2)	Zn	0.6708	0.6828	0.681(40)
Skutterudite	Fe	0.0095	0.0096	0.00948(68)
83 (2)	Co	0.1547	0.1351	0.148(11)
	Ni	0.044	0.0409	0.0440(26)
	As	0.7918	0.8143	0.799(45)
Albite	O	0.4876	0.4842	0.485(47)
81 (7)	Na	0.086	0.0834	0.0855(50)
	Al	0.1034	0.1051	0.1021(59)
	Si	0.3203	0.3234	0.324(18)
	K	0.0018	0.0017	0.00149(47)
	Ca	0.0009	0.0021	0.00148(92)
Almandine	O	0.4201	0.4231	0.425(41)
84 (3)	Mg	0.0645	0.0605	0.0596(34)
	Al	0.1167	0.1192	0.1149(67)
	Si	0.1832	0.1916	0.185(10)
	Ca	0.03	0.027	0.0276(18)
	Mn	0.0046	0.0061	0.00291(22)
	Fe	0.1809	0.1725	0.185(11)
Apatite	O	0.3807	0.4046	0.404(39)
85 (2)	F	0.0377	0.0263	0.0420(30)
	P	0.1842	0.1829	0.177(10)
	Ca	0.3974	0.3862	0.378(21)
Biotite	O	0.4419	0.4460	0.457(44)
91 (1)	Mg	0.1184	0.1245	0.1196(70)
	Al	0.0805	0.0814	0.0778(46)
	Si	0.1820	0.1885	0.179(10)
	K	0.0828	0.0764	0.0798(46)
	Ti	0.0107	0.0113	0.0104(67)
	Fe	0.0838	0.0719	0.0759(51)
BN	B	0.4356	0.5592	0.343(55)
99 (4)	N	0.5644	0.4408	0.657(60)

[a] Spectra measured before 2010.

In Fig. 3 the rhodonite spectra measured before and after the standard re-coating are compared (see Section 2). Assuming a thin film approximation for the conductive coating, the C-K intensity is proportional to the film thickness. For these spectra, the ratio between the intensities of the carbon peaks is 2.7. This value is in agreement with our refinement algorithm, since the ratio between the mean thickness obtained with POEMA for the spectra measured in 2011 and those acquired before 2011 is 2.9 ± 0.4. The corresponding ratio obtained with GENESIS is, instead, 1.33.

5. Conclusions

In the present work, 159 concentration values were obtained, corresponding to 36 standards, by means of the standardless quantification software POEMA. For this set of standards, the performance of POEMA was compared with the commercial software GENESIS Spectrum®. From the 159 values, 26 belong to trace elements, i.e., elements with concentrations less than 1%.

The quantifications performed with POEMA were better than the ones carried out with GENESIS in the 74% of the cases studied. If trace elements were excluded from the data set, the 93% of the concentrations obtained here would present differences relative to the nominal values lower than 10%. Besides the greater accuracy in the obtained concentrations, an important advantage of POEMA is its possibility of refining the conductive coating thickness.

Both software presented important differences with the nominal values in samples containing light elements, such as B, C and N. This discrepancy is mainly due to the uncertainties in the detector efficiency in the low energy region, which is crucial for the determination of concentrations. Thus, a more exhaustive study of the behavior of Si(Li) and silicon drifted detectors for energies lower than 0.4 keV would be of interest. In addition, mass absorption coefficients and certain atomic parameters necessary for the quantification procedure are poorly known for low energies.

Notice that the estimation of uncertainties is a very complex problem. In addition, the criteria used for it are not exempt of certain degree of arbitrariness. For this reason, most of the quantification software do not give any estimation for the errors. The program POEMA, instead, allows the estimation of the uncertainties in the refined parameters, particularly, the mass concentrations. It must be noted that the concentration uncertainties estimated by POEMA were, except for a couple of cases, of the same order of magnitude as the deviations to the nominal values. As expected, the estimated relative uncertainties were greatest for trace elements, up to 40% in most of the cases, while for minor and major constituents the errors were in general lower than 10 and 5%, respectively.

The relative deviations of the concentrations calculated with POEMA with respect to the nominal values were lower than 0.04, for the 66% of the constituents analyzed, while this figure was 0.08 and 0.35 for

Table 2
Mass concentrations obtained with the present method and with the commercial software GENESIS by EDAX compared to the nominal values. Numbers in parentheses are the estimated uncertainties in the two last digits.

Sample Δx_C (nm)	El.	Nom.	EDAX	POEMA
Bustamite	O	0.3841	0.4005	0.398(39)
85 (1)	Na	0.0004	0.0012	0.00040(53)
	Mg	0.0013	0.0024	0.00123(16)
	Si	0.2248	0.2406	0.226(13)
	Ca	0.1353	0.1251	0.1300(74)
	Mn	0.1885	0.1713	0.179 (10)
	Fe	0.0633	0.0577	0.0606(38)
	Zn	0.002	0.0013	0.00500(75)
Chlorite	O	0.5198	0.5093	0.525(51)
88 (2)	Mg	0.2054	0.204	0.197(11)
	Al	0.0973	0.1054	0.1004(60)
	Si	0.1427	0.1471	0.1415(89)
	Cr	0.0068	0.0096	0.00951(88)
	Fe	0.0261	0.0242	0.0250(21)
	Ni	0.0019	0.0004	0.00135(20)
Cr_2O_3	O	0.3157	0.3886	0.356(35)
67 (1)	Cu	0.6843	0.6114	0.644(37)
Cuprite	O	0.1118	0.1364	0.115(11)
74 (1)	Cu	0.8882	0.8636	0.886(50)
Spodumene	O	0.5359	0.524	0.540(53)
86 (1)	Al	0.1506	0.1517	0.1446(85)
	Si	0.3135	0.3243	0.316(18)
Fluorite	F	0.4867	0.4587	0.492(29)
85 (2)	Ca	0.5133	0.5413	0.508(29)
GaAs	Ga	0.482	0.4088	0.437(26)
79 (2)	As	0.518	0.5912	0.536(31)
Pyrope garnet	O	0.4434	0.4465	0.451(44)
84 (2)	Mg	0.1167	0.1214	0.1184(69)
	Al	0.1129	0.1125	0.1097(64)
	Si	0.194	0.2028	0.196(11)
	Ca	0.0332	0.0285	0.0289(20)
	Ti	0.007	0.0064	0.00656(68)
	Cr	0.0039	0.0033	0.00305(55)
	Mn	0.0021	0.0023	0.0021(28)
	Fe	0.0868	0.0763	0.0837(57)
Jadeite	O	0.4735	0.4685	0.478(46)
83 (2)	Na	0.1119	0.105	0.1068(63)
	Al	0.1304	0.1277	0.1248(73)
	Si	0.2771	0.2881	0.282(16)
	Ca	0.0055	0.0069	0.00655(42)
	Fe	0.0016	0.0038	0.00204(16)
Magnetite	O	0.2767	0.294	0.275(27)
86 (1)	Cr	0.0014	0.0018	0.00060(11)
	Fe	0.7219	0.7042	0.724(41)
Ni_2Si	Si	0.193	0.2117	0.187(11)
86 (2)	Ni	0.807	0.7883	0.812(46)
Obsidian	O	0.48845	0.483	0.496(48)
87 (2)	Na	0.03023	0.029	0.0298(18)
	Al	0.06971	0.0702	0.0657(39)
	Si	0.34713	0.3609	0.347(20)
	Cl	0.00362	0.0032	0.00294(30)
	K	0.04198	0.03754	0.0413(26)
	Ca	0.00542	0.00492	0.00500(59)
	Fe	0.01346	0.01124	0.0118(13)
Periclase	O	0.3969	0.4034	0.405(40)
74 (2)	Mg	0.6031	0.5966	0.595(35)
Pyrite	S	0.5345	0.541	0.528(30)
88 (2)	Fe	0.4655	0.459	0.472(27)
Rodonite	O	0.3708	0.3908	0.373(36)
83 (1)	Mg	0.0053	0.0049	0.00468(66)
	Si	0.2146	0.2294	0.221(12)
	Ca	0.0456	0.041	0.0413(24)
	Mn	0.2915	0.2664	0.290(16)
	Fe	0.012	0.0156	0.0122(11)
	Zn	0.0602	0.052	0.0586(74)
Sanidine	O	0.4635	0.4552	0.467(45)
82 (1)	Na	0.0223	0.0226	0.0243(15)
	Al	0.0995	0.1036	0.0984(57)
	Si	0.3028	0.3171	0.308(17)
	K	0.1007	0.0887	0.0955(55)
	Fe	0.0014	0.0015	0.0013(33)
	Ba	0.0098	0.0113	0.00574(69)

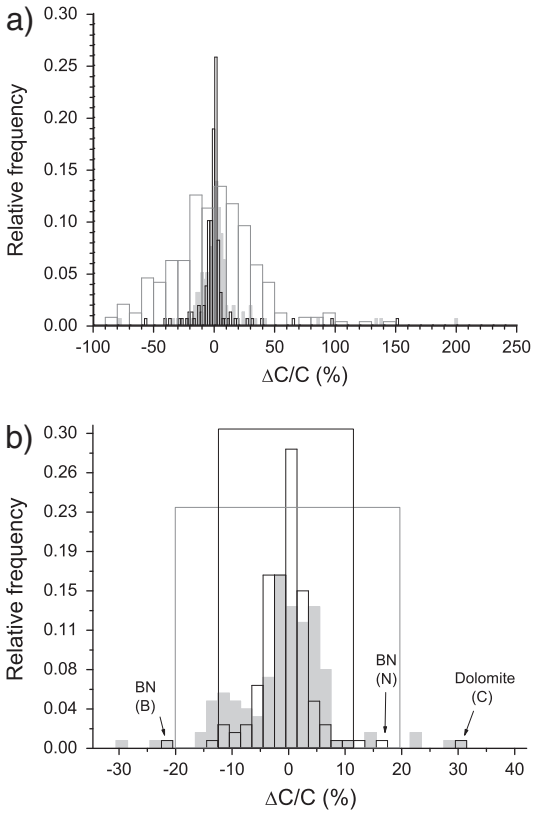

Fig. 2. Histograms of the differences of concentrations relative to the nominal values obtained in this work by means of the standardless quantification programs POEMA (black hollow bars) and GENESIS Spectrum® (gray full bars). a) Results obtained by Newbury et al. [2] for the quantification with the DTSA program for other set of samples (gray hollow bars) are also included. b) Histogram obtained by excluding trace elements (concentrations less than 1%). The black and gray rectangular frames comprise the 95% of the cases for POEMA and GENESIS, respectively.

GENESIS and DTSA, respectively. This improvement allows us to state that the results obtained with the standardless algorithm of quantification presented here were reliable within a good degree of accuracy.

Acknowledgments

The authors acknowledge *Universidad Nacional de Córdoba* and *Consejo Nacional de Investigaciones Científicas y Técnicas* from the República Argentina for financial support. Measurements were performed in the *rotect Laboratorio de Microscopía Electrónica y*

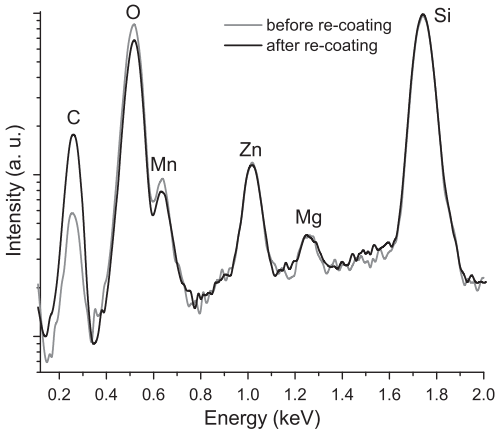

Fig. 3. Effects of the variation of conductive coating. Spectra corresponding to the rhodonite mineral standard measured before (gray line) and after (black line) the standard re-coating.

Microanálisis (LABMEM) from the *Universidad Nacional de San Luis*, Argentina.

Appendix A. Supplementary data

Supplementary data to this article can be found online at http://dx.doi.org/10.1016/j.sab.2012.08.003.

References

[1] J. Goldstein, D. Newbury, D. Joy, C. Lyman, P. Etchling, E. Lifshin, L. Sawyer, J. Michael, Scanning Electron Microscopy and X-ray Microanalysis, 3rd ed. Springer, New York, 2007.
[2] D. Newbury, C. Swyt, R. Myklebust, "Standardless" quantitative electron probe microanalysis with energy-dispersive X-ray spectrometry: is it worth the risk? Anal. Chem. 67 (1995) 1866–1871.
[3] C. Merlet, Capability and uncertainty of standardless procedures for quantitative electron probe X-ray microanalysis, Microsc. Microanal. 9 (2003) 524–525.
[4] J. Trincavelli, R. Van Grieken, Peak-to-background method for standardless electron microprobe analysis of particles, X-Ray Spectrom. 23 (1994) 254–260.
[5] J. Lábár, S. Török, A peak-to-background method for electron probe X-ray microanalysis applied to individual small particles, X-Ray Spectrom. 21 (1992) 183–190.
[6] H. Wagner, W. Werner, Calculation of ionization depth distributions and backscattering coefficients applying a new Monte Carlo simulation approach, X-Ray Spectrom. 27 (1998) 373–380.
[7] J.S.B. Reed, Electron Microprobe Analysis and Scanning Electron Microscopy in Geology, Cambridge University Press, Cambridge, 1996.
[8] D. Newbury, Standardless quantitative electron-excited X-ray microanalysis by energy-dispersive spectrometry: what is its proper role? Microsc. Microanal. 4 (1999) 585–597.
[9] J. Pouchou, Standardless X-ray analysis of bulk specimens, Microchim. Acta 114 (1994) 33–52.
[10] C. Campos, M.A.Z. Vasconcellos, J. Trincavelli, S. Segui, Analytical expression for K- and L-shell cross sections of neutral atoms near ionization threshold by electron impact, J. Phys. B: At. Mol. Opt. Phys. 40 (2007) 3835–3841.
[11] R. Bonetto, G. Castellano, J. Trincavelli, Optimization of parameters in electron probe microanalysis, X-Ray Spectrom. 30 (2001) 313–319.
[12] G. Castellano, R. Bonetto, J. Trincavelli, M.A.Z. Vasconcellos, C. Campos, Optimization of K-shell intensity ratios in electron probe microanalysis, X-Ray Spectrom. 31 (2002) 184–187.
[13] J. Trincavelli, G. Castellano, R. Bonetto, L-shell transition rates for Ba, Ta, W, Pt, Pb and Bi using electron microprobe, Spectrochim. Acta Part B 57 (2002) 919–928.
[14] S. Limandri, J. Trincavelli, R. Bonetto, A. Carreras, Structure of the Pb, Bi, Th and U M X-ray spectra, Phys. Rev. A: At. Mol. Opt. Phys. 78 (2008) 1–10 022518.
[15] S. Limandri, R. Bonetto, A. Carreras, J. Trincavelli, S. Limandri, R. Bonetto, A. Carreras, J. Trincavelli, Kα satellite transitions in elements with $12 \leq Z \leq 30$ produced by electron incidence, Phys. Rev. A: At. Mol. Opt. Phys. 82 (2010) 1–9 (032505).
[16] S. Limandri, A. Carreras, R. Bonetto, J. Trincavelli, Kβ satellite and forbidden transitions in elements with $12 \leq Z \leq 30$ induced by electron impact, Phys. Rev. A: At. Mol. Opt. Phys. 81 (2010) 1–9 (012504).
[17] G. Castellano, J. Osán, J. Trincavelli, Analytical model for the bremsstrahlung spectrum in the 0.25–20 keV photon energy range, Spectrochim. Acta Part B 59 (2004) 313–319.
[18] J. Trincavelli, G. Castellano, The prediction of thick target electron bremsstrahlung spectra in the 0.25–50 keV energy range, Spectrochim. Acta Part B 63 (2008) 1–8.
[19] C. Visñovezky, S. Limandri, M.E. Canafoglia, R. Bonetto, J. Trincavelli, Asymmetry of characteristic X-ray peaks obtained by a Si(Li) detector, Spectrochim. Acta Part B 62 (2007) 492–498.
[20] S. Limandri, R. Bonetto, H. Di Rocco, J. Trincavelli, Fast and accurate expression for the Voigt function. Application to the determination of uranium M linewidths, Spectrochim. Acta Part B 63 (2008) 962–967.
[21] J. Trincavelli, S. Limandri, A. Carreras, R. Bonetto, Experimental method to determine the absolute efficiency curve of a wavelength dispersive spectrometer, Microsc. Microanal. 14 (2008) 306–314.
[22] S. Limandri, A. Carreras, J. Trincavelli, Effects of the carbon coating and the surface oxide layer in electron probe microanalysis, Microsc. Microanal. 16 (2010) 583–593.
[23] J.H. Hubbell, Bibliography and Current Status of K, L, and Higher Shell Fluorescence Yields for Computations of Photon Energy-Absorption Coefficients, in: NISTIR National Institute of Standards and Technology, Gaithersburg, MD, 1989, pp. 89–4144.
[24] J. Riveros, G. Castellano, J. Trincavelli, Comparison of $\phi(\rho z)$ curve models in EPMA, Microchim. Acta 12 (1992) 99–105.
[25] R. Packwood, J. Brown, A Gaussian expression to describe $\phi(\rho z)$ curves for quantitative electron probe micro- analysis, X-Ray Spectrom. 10 (1981) 138–146.
[26] J.A. Bearden, X-ray wavelengths, Rev. Mod. Phys. 39 (1967) 78–124.
[27] M. Pia, P. Saracco, M. Sudhakar, Validation of K and L shell radiative transition probability calculations, IEEE Trans. Nucl. Sci. 56 (2009) 3650–3661.
[28] D. Joy, Fundamental constants for quantitative X-ray microanalysis, Microsc. Microanal. 7 (2001) 159–167.
[29] L. Smith, Thin-Film Deposition: Principles and Practice, McGraw-Hill Proffessional, 1995.
[30] C.T. Chantler, K. Olsen, R.A. Dragoset, J. Chang, A.R. Kishore, S.A. Kotochigova, D.S. Zucker, X-ray form factor, attenuation and scattering tables (version 2.1), 2005, http://physics.nist.gov/ffast, National Institute of Standards and Technology, Gaithersburg, MD. Originally published as C. T. Chantler, X-ray form factor, attenuation, and scattering tables, J. Phys. Chem. Ref. Data 29 (2000) 597–1048;
C.T. Chantler, Theoretical form factor, attenuation, and scattering tabulation for $Z = 1–92$ from $E = 1–10$ eV to $E = 0.4–1.0$ MeV, J. Phys. Chem. Ref. Data 24 (1995) 71–643.
[31] J.L. Campbell, Fluorescence yields and Coster–Kronig probabilities for the atomic L subshells, At. Data Nucl. Data Tables 85 (2003) 291–315.
[32] J.L. Campbell, Fluorescence yields and Coster–Kronig probabilities for the atomic L subshells. Part II: the L1 subshell revisited, At. Data Nucl. Data Tables 95 (2009) 115–124.
[33] J. Campbell, A Report Prepared for the International Initiative on X-ray Fundamental, University of Canberra, http://www.canberra.edu.au/irps/archives/vol24no1/xray.pdf (accessed December 1, 2011).
[34] S. Limandri, Optimización de parámetros en microanálisis con sonda de electrones. Aplicación a la cuantificación sin estándares, Ph.D Dissertation, Universidad Nacional de Córdoba, 2011, http://www.famaf.unc.edu.ar/publicaciones/publicaciones.html#publ-serie-d-fisica.
[35] S. Limandri, M.A.Z. Vasconcellos, R. Hinrichs, J. Trincavelli, Experimental determination of K-shell ionization cross sections by electron impact for C, O, Al, Si and Ti, unpublished results.
[36] Natl. Institute of Standards and Technology — Natl. Institutes of Health, http://www.cstl.nist.gov/div837/Division/outputs/DTSA/DTSA.htm (accessed August 15, 2011).
[37] S.J.B. Reed, Electron Microprobe Analysis, 2nd. ed. Cambridge University Press, Cambridge, 1993.